7916 *Biochemistry* **2009,** *48,* 7916–7926
DOI: 10.1021/bi9003952

BIOCHEMISTRY
including biophysical chemistry & molecular biology
Article

Novel Domain Arrangement in the Crystal Structure of a Truncated Acetyl-CoA Synthase from *Moorella thermoacetica*[†,‡]

Anne Volbeda,*[,§] Claudine Darnault,[§] Xiangshi Tan,[∥,§] Paul A. Lindahl,[∥] and Juan C. Fontecilla-Camps*[,§]

[§]*Laboratoire de Cristallographie et Cristallogenèse des Protéines, Institut de Biologie Structurale Jean-Pierre Ebel, CEA, CNRS, Université Joseph Fourier, 41 Rue Jules Horowitz, F-38027 Grenoble, France,* [∥]*Departments of Chemistry and of Biochemistry and Biophysics, Texas A&M University, College Station, Texas 77843, and* [§]*Current address: Department of Chemistry, Institute of Biomedical Sciences, Fudan University, Shanghai, 200043, P.R. China*

Received March 9, 2009; Revised Manuscript Received June 26, 2009

ABSTRACT: Ni-dependent acetyl-CoA synthase (ACS) and CO dehydrogenase (CODH) constitute the central enzyme complex of the Wood−Ljungdahl pathway of acetyl-CoA formation. The crystal structure of a recombinant bacterial ACS lacking the N-terminal domain that interacts with CODH shows a large reorganization of the remaining two globular domains, producing a narrow cleft of suitable size, shape, and nature to bind CoA. Sequence comparisons with homologous archaeal enzymes that naturally lack the N-terminal domain show that many amino acids lining this cleft are conserved. Besides the typical [4Fe-4S] center, the A-cluster contains only one proximal metal ion that, according to anomalous scattering data, is most likely Cu or Zn. Incorporation of a functional $Ni_2Fe_4S_4$ A-cluster would require only minor structural rearrangements. Using available structures, a plausible model of the interaction between CODH and the smaller ACS in archaeal multienzyme complexes is presented, along with a discussion of evolutionary relationships of the archaeal and bacterial enzymes.

Ni-dependent acetyl-coenzyme A synthase (ACS)[1] is a NiFeS-cluster enzyme that requires strict anoxic conditions to function. In the acetogenic bacterium *Moorella thermoacetica* (*Mot*), the ACS α-subunit forms an $\alpha_2\beta_2$ heterotetramer with the Ni-containing carbon monoxide dehydrogenase (CODH) β-subunit (*1*). This association constitutes the central enzyme complex of the anaerobic Wood−Ljungdahl pathway of acetyl-CoA synthesis from CO_2 (*2*, *3*). The structure of this complex is known in two crystal forms (*4*, *5*) and shows a long hydrophobic tunnel network that allows the CO produced at the CODH active site, the C-cluster, to be used at the ACS active site, the A-cluster, without being released to the medium. Our understanding of CO_2 reduction to CO by CODH has progressed significantly thanks to the recent crystal structures of key catalytic intermediates in the homodimeric β_2 enzyme from *Carboxydothermus hydrogenoformans* (*Ch*) (*6*) and the heterotetrameric $\alpha_2\varepsilon_2$ enzyme from the archaeon *Methanosarcina barkeri* (*Meb*) (*7*) (see also ref *8*). However, many mechanistic details of acetyl-CoA formation by ACS have not yet been elucidated. The active A-cluster has been characterized as a $Ni_2Fe_4S_4$ center in the crystal structures of both bifunctional CODH/ACS_{Mot} and monofunctional ACS_{Ch} (*5*, *9*), in agreement with many previous studies, as reviewed in refs *10* and *11*. Catalysis involves three substrates, CoA, CO, and the cobalt-containing methyl-carrying corrinoid iron−sulfur protein (CoFeSP):

$$CoAS^- + CO + CH_3{}^- - Co(III)FeSP \rightleftarrows CoA - SC(O)CH_3 + Co(I)FeSP$$

At least five steps take place at the A-cluster during catalysis: (i) binding of CO, (ii) transfer of the methyl group from CoFeSP, (iii) formation of an acetyl intermediate, (iv) binding of CoA, and (v) formation of acetyl-CoA. In addition, ACS requires reductive activation (*12*). This is so because the methyl group is provided by CoFeSP as a $CH_3{}^+$ cation (*13*), and two electrons are required to form a carbon−metal bond, most likely with the proximal Ni ion of the A-cluster. The two electrons are recovered upon reductive elimination of the acetyl intermediate to form acetyl-CoA. So far, crystal structures of well-defined catalytic intermediates of ACS have not been reported.

Here we report the crystallographic analysis of a truncated form of ACS_{Mot}, with a molecular mass of 49 kDa called α_{49} (*14*). Because it lacks the 310 residue long N-terminal domain, α_{49} resembles the homologous ACS β-subunit of the acetyl-CoA decarbonylase/synthase (ACDS) multienzyme complex found in methanogenic archaea. To avoid confusion, we will use the nomenclature *A1*, *A2*, and *A3* for ACS domains and *C1*, *C2*, etc. for CODH domains, regardless of their origin. In ACS_{Mot}, *A1* is involved in extensive intersubunit interactions with CODH and contains a significant part of the hydrophobic tunnel that connects the C- and A-clusters (*4*, *5*). The isolated, recombinant archaeal ACS can be activated by adding $NiCl_2$. According to metal analyses and spectroscopic studies, the reconstituted *Methanosarcina thermophila* (*Met*) ACS contains, like its bacterial counterparts, a classical $Ni_2Fe_4S_4$ A-cluster (*15*−*17*). The

[†]This study was supported by institutional funding from the CEA and the CNRS and by the National Institutes of Health (GM046441 to P.A.L.).
[‡]The atomic coordinates and structure factors (accession number 3GIT) have been deposited in the Protein Data Bank, Research Collaboratory for Structural Bioinformatics (http://www.pdb.org).
*To whom correspondence should be addressed. A.V.: tel, +33438789606; fax, +33438785122; e-mail, anne.volbeda@ibs.fr. J.C. F.-C.: tel, +33438785920; fax, +33438785122; e-mail, juan.fontecilla@ibs.fr.
[1]Abbreviations: ACS, acetyl-CoA synthase; ACDS, acetyl-CoA decarbonylase/synthase; *Ch, Carboxydothermus hydrogenoformans*; CoA, coenzyme A; CoFeSP, corrinoid iron−sulfur protein; CODH, carbon monoxide dehydrogenase; HCP, hybrid cluster protein; *Meb*, *Methanosarcina barkeri*; *Met*, *Methanosarcina thermophila*; *Mot*, *Moorella thermoacetica*.

 Published on Web 07/13/2009

ACDS complex also contains $\gamma\delta$ CoFeSP heterodimers and $\alpha_2\varepsilon_2$ heterotetramers, with α_2 corresponding to CODH (*18*). It has been shown that the hydrophobic tunnels of both the bacterial and the archaeal enzymes can bind xenon (*5*, *7*, *19*). The absence of the bacterial tunnel-containing *A1* domain in archaeal ACS raises the question how CO diffuses between the A- and C-clusters in the archaeal ACDS complex.

The crystal structure of ACS_{Mot} has been determined in closed (α_C) and open (α_O) conformations (*5*). The difference between the two structures is due to a large movement of *A1*, which in α_O blocks the connection between the A-cluster, bound to domain *A3*, and the tunnel network (*5*, *20*). Conversely, when the enzyme is in the α_C conformation, the A-cluster can bind the CO produced at the C-cluster, because the connection to the hydrophobic tunnel network is open. Only inactive $NiCuFe_4S_4$ and $NiZnFe_4S_4$ A-clusters have been found in crystal structures of this form (*4*, *5*). Functional $Ni_2Fe_4S_4$ A-clusters (*10*, *11*) have been observed in two α_O crystal structures, where the A-cluster is exposed to the medium (*5*, *9*). Therefore, the enzyme is likely to accept the methyl group from CoFeSP when it is in the α_O conformation. When the enzyme is treated with exogenous CO, a Ni(I)−CO complex is formed. Furthermore, ^{57}Fe, ^{59}Ni, and ^{13}C isotopic labeling experiments have shown that Ni, CO, and the [4Fe-4S] cluster interact magnetically, giving rise to an EPR spectrum known as the NiFeC signal (refs *10* and *11* and references cited therein).

Purified recombinant α_{49} contains ~4 Fe and 0.5 Ni per A-cluster (*14*). Incubation with $NiCl_2$ followed by reduction with dithionite and exposure to CO yielded an EPR signal reminiscent of NiFeC in terms of *g*-values and relaxation/saturation properties. The ability to generate this pseudo-NiFeC signal indicates that an A-cluster derivative can be reconstituted in the truncated subunit. The spin concentration of this signal was only ~25% of that normally observed for NiFeC, and the truncated subunit had no catalytic activity. In this respect, α_{49} resembles other constructs of the *Mot* enzyme, where metal heterogeneity at the active site and substoichiometric amounts of nickel are a recurrent problem. The α_{49} structure presented here contains a novel metal-containing inactive form of the A-cluster and a new arrangement of domains *A2* and *A3*. We will call this form $\alpha_{49(T)}$. Below, we will discuss the relevance of these findings with respect to previous studies on the activity of bacterial and archaeal ACS's. We will also address the possible evolutionary implications of the striking similarities between ACS and CODH domains.

MATERIALS AND METHODS

Crystallization. α_{49}, a 49 kDa fragment of ACS_{Mot}, was purified after heterologous expression in *Escherichia coli*, as previously described (*14*). It contains residues 311−729 of the intact enzyme and a C-terminal His tag. All crystallization experiments were performed at room temperature in an anaerobic glovebox, using the vapor diffusion method. Crystals with maximal dimensions of $0.3 \times 0.3 \times 0.2$ mm^3 were obtained after 6−8 weeks. The best ones grew in hanging drops that were prepared by mixing 1 μL of a solution with a protein concentration of 20 mg/mL and 2 mM sodium dithionite in 50 mM Tris-HCl at pH 8.0, with 1 μL of a reservoir solution containing 1.4 M ammonium sulfate (AS), 2 mM sodium dithionite, and 100 mM Tris-HCl at pH 7.1. After transfer to a stabilization solution containing 2.2 M AS and 30% glycerol, in addition to the other reservoir components, crystals were flash-cooled inside the glovebox in liquid propane and subsequently stored in liquid nitrogen, as described (*21*).

Table 1: Crystallographic Statistics for the Truncated ACS Crystal Structure

data		refinement	
space group	$P3_121$	resolution (Å)	20.0−3.0
cell dimensions		reflections in work set	74440
a, *b* (Å)	166.4	R_{work} (%)	17.1
c (Å)	245.2	reflections in test set	3902
molecules/asymmetric unit	6	R_{free} (%)	20.8
resolution (Å)[a]	20−3 (3.1−3.0)	total no. of atoms	20121
R_{sym} (%)[a]	5.3 (24.3)	water molecules	161
$\langle I\rangle/\langle\sigma(I)\rangle$[a]	19.6 (6.3)	sulfate molecules	24
no. of observations[a]	588420 (55207)	glycerol molecules	6
unique reflections[a]	78314 (7323)	σ_{bond} (Å)	0.015
completeness (%)[a]	99.5 (99.7)	σ_{angle} (deg)	1.59
		average *B* factor (Å^2)	57.3

[a] Numbers in parentheses refer to the highest resolution shell.

X-ray Data Collection and Processing. Diffraction data were collected to 3.0 Å resolution on a MAR CCD165 detector (MAR Research, Germany) by exposing the best crystal to monochromatic (λ = 1.008 Å) X-rays under a cold (≈100 K) nitrogen stream. A total of 450 images were collected with 0.4° oscillations, using the BM30A beamline of the European Synchrotron Radiation Facility in Grenoble, France. Diffraction spots were integrated, scaled, subjected to a zero-dose correction (*22*), and reduced to structure factor amplitudes with XDS (*23*). The first 333 images were selected to produce 99.5% complete data with good intensity statistics (Table 1). The crystal belonged to the trigonal space group $P3_121$ with cell dimensions $a = b = 166.4$ Å and $c = 245.2$ Å. A similar but less well diffracting crystal with a halved crystallographic *c*-axis was used to collect data to 3.7 Å resolution at the high energy side of the Ni absorption edge (λ = 1.4827 Å). These data were used to check the presence of Ni (statistics not shown).

Structure Solution. The phase problem was solved by molecular replacement with Phaser (*24*−*26*), using the 3 Å resolution data and domains *A2* and *A3* of ACS_{Mot} α_O as search models. For success, it was necessary to exclude the N-terminal region of domain 2 (residues 311−319) and a long interdomain helix (residues 471−499). In addition, low peaks from the rotation function output had to be included in order to find well-contrasting solutions in the translation search. Checks with anomalous difference maps showed that good solutions gave strong peaks for the A-cluster. The asymmetric unit contains six molecules related by noncrystallographic symmetry (ncs) operations close to those of a regular 32 hexamer and a solvent content of about 63%. In the crystal with the smaller unit cell, which contains a trimer per asymmetric unit, the 2-fold axes of the hexamer correspond to crystallographic symmetry operations.

Refinement. Because of the limited data resolution, refinement was carried out with tight ncs restraints, using REFMAC (*27*, *28*) and including TLS refinement (*29*) to model overall anisotropic displacements of the 12 domains present in the hexamer. Manual model corrections were performed with the TURBO computer graphics package (*30*). The quality of electron density maps was significantly improved by averaging, using the program SUPERMAP (*31*). A first 6-fold averaged electron density map obtained with molecular replacement phases clearly

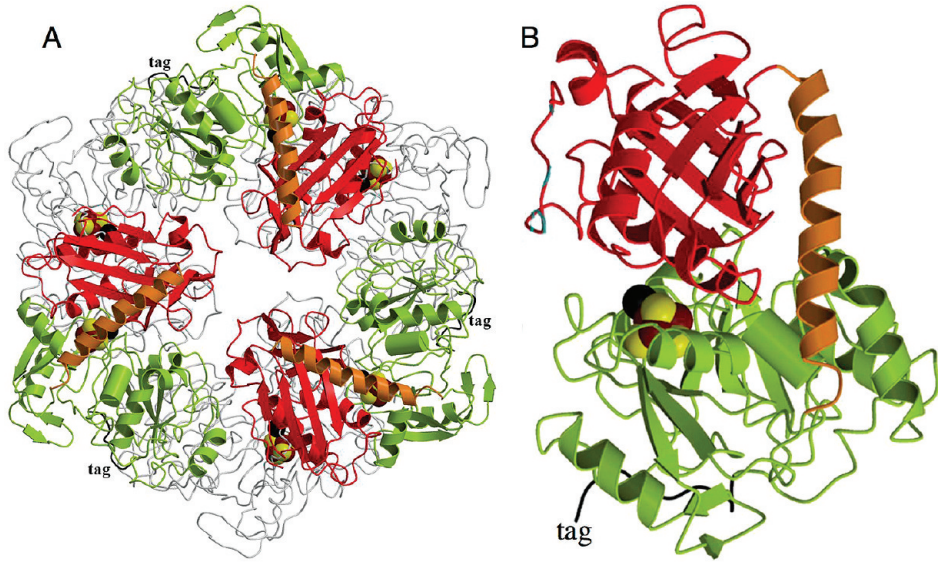

FIGURE 1: Polypeptide fold of α_{49} in the new $\alpha_{49(T)}$ conformation. (A) Hexamer. (B) Monomer. Domain *A2* is shown in red, domain *A3* in lime green, the connecting α-helix in orange, and the C-terminal His tag in black. A-cluster atoms are depicted as brown (Fe), yellow (S), and black (Zn or Cu) spheres. The bottom trimer in (A) is shown as a gray C_α trace.

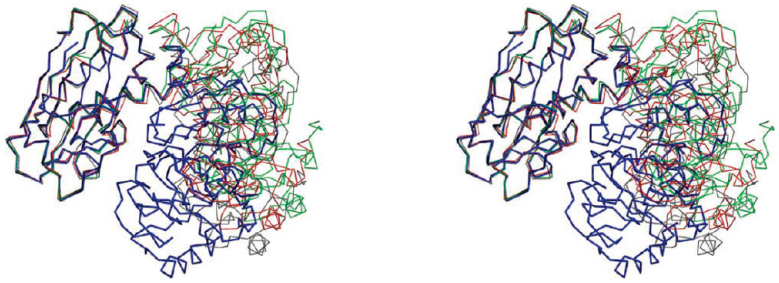

FIGURE 2: Stereo image of ACS C_α backbone superposition of *Mot* $\alpha_{49(T)}$ (blue), α_O (green), and α_C (red) and of *Ch* α_O (gray) to domain *A2*, excluding domain *A1*.

showed the long helix between domains *A2* and *A3* that was left out of the starting model. Part of the main chain of the C-terminal His tag also appeared in this map, at the dimer interfaces of the hexamer (Figure 1), but the corresponding side chains were only partially resolved during refinement. The first six N-terminal residues of $\alpha_{49(T)}$ are disordered and therefore were not included in the model. Refinement statistics of the final model are given in Table 1.

Structure and Sequence Analyses. Figures 1−3, 5, 7, 8, and S2 were prepared with the programs MOLSCRIPT (*32*) and RASTER3D (*33*), in addition to CONSCRIPT (*34*) that was used for the display of electron density maps (Figure 3). The electrostatic potential surfaces of Figure 4 were determined at pH 7 with the APBS (*35*) plugin of PyMOL (http://www.pymol.org), after addition of hydrogen atoms with PDB2PQR (*36*) using the AMBER force field (*37*) and pK_a's calculated with PROPKA (*38*), excluding the metal and inorganic sulfur atoms of the A-cluster from the protein. Structural superpositions were performed with the BIOMOL program SUPPOS (http://www.xray.chem.rug.nl/Links/Biomol1.htm). Tunnels and cavity maps in Figures 5, 7, 8, and S2 were calculated with the program CAVsel (A. Volbeda, unpublished). Amino acid sequences used in the manual structure-based alignments in Figures 6 and S1 were obtained from SWISSPROT (http://www.ebi.ac.uk/swissprot/).

RESULTS

Crystal Structure Determination. The structure of α_{49} in the novel $\alpha_{49(T)}$ conformation has been solved at 3.0 Å resolution by molecular replacement (Table 1). There is a regular trimer of dimers in the asymmetric unit (Figure 1). A similar crystal form with an approximately halved *c*-axis contained a trimer in the asymmetric unit and diffracted to 3.7 Å resolution. After refinement of the 3.0 Å resolution structure, an average temperature factor of 57.3 Å^2 was obtained, suggesting small differences in subunit orientations between hexamers. The final model shows good refinement statistics (Table 1), as indicated by a satisfactory geometry and an R_{free} of 20.8% for all structure factor observations between 20 and 3.0 Å resolution. Although we were unable to obtain X-ray data to a better resolution, precluding a detailed study with $\alpha_{49(T)}$, the model is of sufficient quality to allow the analysis of both fold and major active site differences with previously obtained structures.

Changes with Respect to Previous ACS Structures. In $\alpha_{49(T)}$, domains *A2* and *A3* have significantly moved to each other relative to their previously known conformations (Figure 2). This movement corresponds to a rotation around a hinge region located close to the C-terminus of the long interdomain helix (residues 471−499, shown in orange in Figure 1). The internal structure of the two domains in the new conformation does not change much: separate C_α superpositions of domains *A2* (residues 318−491) and *A3* (residues 494−729) of $\alpha_{49(T)}$ to those of α_O give root-mean-square deviations (rmsd's) of about 0.5 Å. Taking *A2* as a reference (Figure 2), the structural change of $\alpha_{49(T)}$ with respect to α_O may be described as a rotation (κ) of domain *A3* by 50° and a translation parallel to the rotation axis

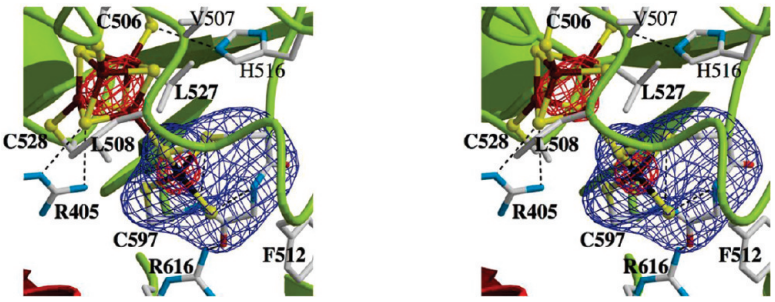

FIGURE 3: Stereo image of the active site in $\alpha_{49(T)}$. The blue grid depicts a 6-fold averaged $F_o - F_c$ electron density map with the metal site next to the [4Fe-4S] cluster and its protein ligands (Cys509Cβ and Sγ, Cys595Cα to Cys597Sγ) omitted from the phase and structure factor calculations. The red grid corresponds to a 6-fold averaged 3.0 Å resolution anomalous difference map.

($T_{\|}$) of 4.6 Å, with a maximal shift of 34 Å in C_α positions. Although the domain conformation of $\alpha_{49(T)}$ is somewhat closer to that of α_O in ACS_{Ch} (*9*), after superposition of their respective *A2* domains there is still a substantial difference in the position of domain *A3* ($\kappa = 35°$, $T_{\|} = 1.3$ Å). Our results indicate that there is much more flexibility in the relative positions of domains *A2* and *A3* than previously recognized (Figure 2). In fact, the rearrangement of domain *A*3 in $\alpha_{49(T)}$ is as extensive as the one observed for domain *A1* between α_C and α_O in ACS_{Mot} (*5*). When the corresponding *A2* domains are superimposed, there are no bad clashes between α_O *A1* and $\alpha_{49(T)}$ *A3*. However, the superposition of α_C to $\alpha_{49(T)}$ leads to the collision of these two domains (not shown). It follows that the $\alpha_{49(T)}$ conformation is compatible with the orientation of *A1* in α_O, but not in α_C.

At the X-ray wavelength of 1.008 Å used for data collection with the best $\alpha_{49(T)}$ crystal, a map calculated with $\triangle_{anom}$ coefficients displayed high peaks at the active site for both the [4Fe-4S] cluster and one metal ion (Figure 3). This ion occupies the proximal site relative to the cluster, previously called M_p (*5*). An equivalent map was calculated with 3.7 Å resolution data collected at $\lambda = 1.4827$ Å from the related crystal with the smaller unit cell. In this map, the peak corresponding to the [4Fe-4S] cluster was still present, but there was no peak at M_p (not shown). Thus, there is no evidence for the presence of Ni in the A-cluster in $\alpha_{49(T)}$. Because (i) the λ used is lower than the wavelength corresponding to the Ni absorption edge and (ii) there is a high electron density peak at M_p in the map calculated with $2F_o - F_c$ coefficients, it appears that a metal ion heavier than nickel occupies the proximal site. The most likely candidates are Cu and Zn, as these metals were also observed in previous crystal structures of ACS_{Mot} (*4*, *5*). A flat $F_o - F_c$ difference map for the ion at M_p was obtained with 75% occupied Zn^{2+}. The metal ion is tetrahedrally coordinated by an external ligand, modeled as HS^- with the same occupancy, and by the thiolate groups of Cys509, Cys595, and Cys597 (Figure 3).

The cleft formed between $\alpha_{49(T)}$ domains *A2* and *A3* is located opposite to where *A1* would be in the enzyme. An analysis of electrostatic potential surfaces (Figure 4) strongly suggests that this cleft may bind the highly negatively charged (*39*) CoA substrate and acetyl-CoA product: it contains the most extensive complementary positive charge distribution of the truncated structure, which is located mainly on the surface of *A2*. The same positive patch is visible in the structures of α_O (Figure 4A) and α_C (Figure 4B), but in these conformations it is approximately twice as far away from the A-cluster than in $\alpha_{49(T)}$. Only in the latter conformation (Figure 4C) does the distance of about 15 Å between the patch and the A-cluster seem compatible with functional binding of the coenzyme.

Results from fluorescence quenching, chemical modification, and protection experiments led Wood and co-workers to propose that CoA binding to ACS protects about five tryptophan residues and two arginines from chemical modification (*40*, *41*): (i) the modification of these residues causes the loss of the $^{13}CO/CO$ exchange reaction in acetyl-CoA catalyzed by the A-cluster; (ii) modification of the arginines modifies the fluorescence of the tryptophan(s) indicating that some are close to each other; (iii) at least one of the modified tryptophans must be close to the A-cluster because it perturbs the NiFeC EPR signal; (iv) both adenine and 3′-dephospho-CoA quench the tryptophan residue-(s) fluorescence, suggesting that the 3′-phosphate group is not essential for CoA binding; (v) the pyrophosphate bridge of CoA binds to arginine(s) as indicated by the protection that added pyrophosphate exerted against the chemical modification of these residues; and (vi) these modifications only affect the microenvironment around the targeted residues, as shown by CD. The cleft formed between *A2* and *A3* contains two tryptophans, 418 and 427, and four arginines, 334, 346, 429, and 616 (Figure 5A). Trp418 is likely to be one of the modified residues because in $\alpha_{49(T}$ it is the closest tryptophan to the A-cluster at 12.5 Å, and consequently, it could influence the NiFeC signal. Trp427 may be also a potential candidate for chemical modification being at 17.5 Å from the A-cluster. Consistent with the results described above (v), arginines 334, 346, 429, and 616 are close to the two tryptophans.

Coenzyme A could be stabilized through interactions of (i) the adenine ring with Trp418 or Trp427 and (ii) its pyrophosphate region with the guanidinum group of two of the arginines mentioned above (Figure 5A). These interactions are also compatible with the approach of the cysteamine moiety of the coenzyme to the M_p site of the A-cluster through a narrow tunnel that does not exist in the other α-subunit conformations (Figure 5B). Assisted by His419, His408 may abstract a proton from CoA-SH before its putative binding to the apical binding site of Ni_p (labeled with *). Next, it may react with an acetyl group bound equatorially to Ni_p (at the site labeled with $). A cavity above the S atom of the coenzyme shows that there is also enough space for the acetyl-CoA product. We conclude that, if $\alpha_{49(T)}$ has functional relevance, it may approximate the CoA binding conformation of ACS. The fact, as mentioned above, that the $\alpha_{49(T)}$ conformation is incompatible with α_C is not surprising because the acetylated ACS, that binds CoA, should not be able to adopt this conformation due to steric hindrance at the A-cluster.

Comparison to Archaeal Enzymes. In order to investigate whether the domain arrangement in $\alpha_{49(T)}$ could arise from crystal packing interactions, we compared the amino acid

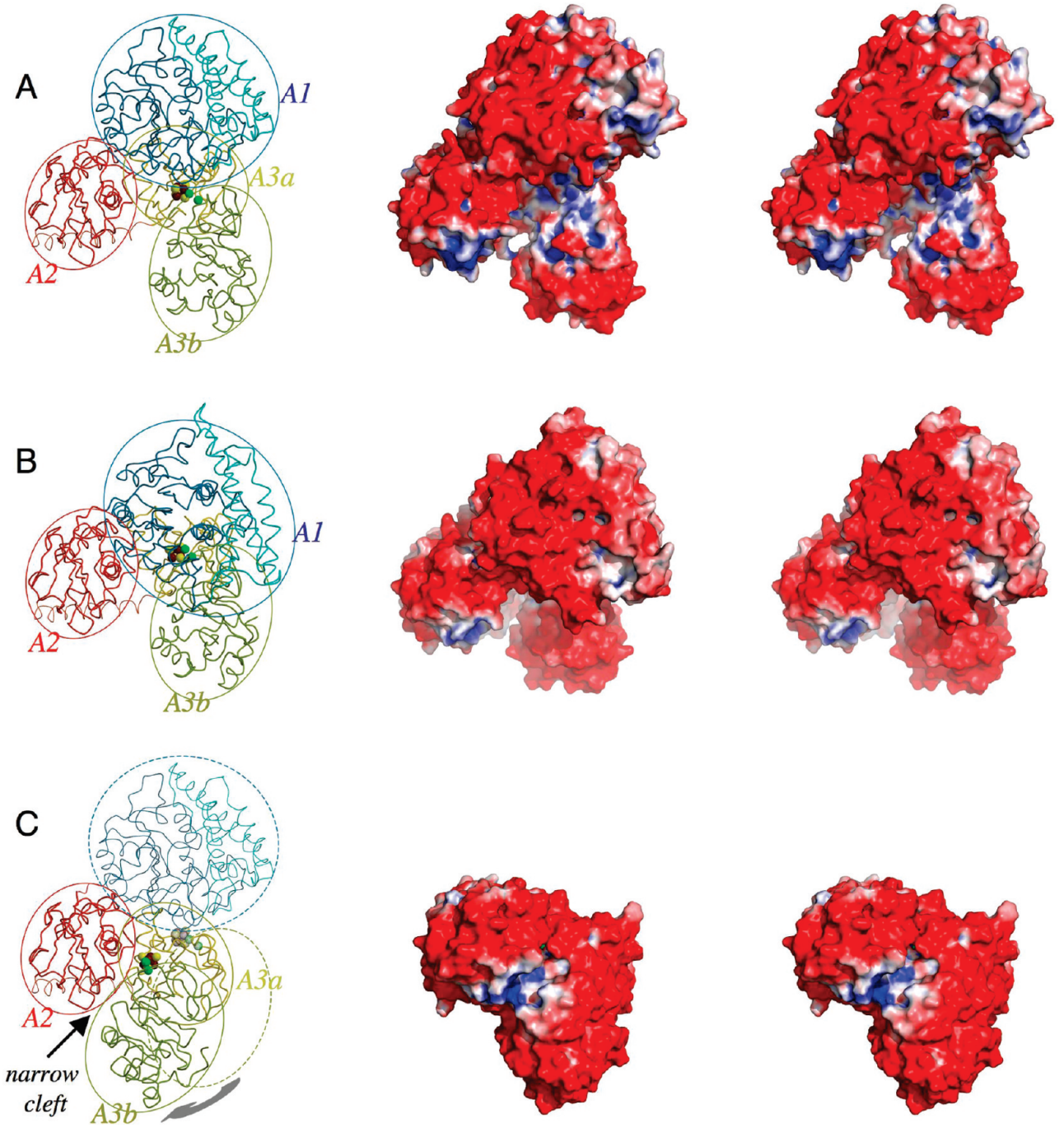

FIGURE 4: Relative domain movements and stereo images of electrostatic potential surfaces of three ACS_{Mot} structures after superposition of their respective *A2* domains: (A) α_O; (B) α_C; (C) $\alpha_{49(T)}$. Domains are shown as thin ribbons, and they are labeled *A1*, *A2*, *A3a*, and *A3b*, with dashed ellipsoids showing their positions in α_O. In (C) the hypothetical position of *A1* is depicted in light blue, with the A-cluster position in α_O shown in semitransparent mode. Color code of the electrostatic potential surfaces: red, negative; blue, positive.

sequences of the two bacterial enzymes of known structure with two methanogenic (*Met* and *Meb*) counterparts. Out of the 403 aligned residues, 147, or 36.4%, are invariant (Figure 6), suggesting that the bacterial and archaeal ACS's have very similar structures. Out of the 30 residues involved in interactions ($d < 3.8$ Å) between domains *A2* and *A3* in $\alpha_{49(T)}$, 18, or 60%, are invariant. By comparison, only 13 residues are involved in *A2*/*A3* contacts in both α_O and α_C. Seven of these residues, or 54%, are invariant and 6 of them are also involved in *A2*/*A3* interactions in $\alpha_{49(T)}$. If the conformation of the latter were a crystallization artifact, the fraction of invariant residues involved in its domain interactions would not be expected to be higher than the overall 36.4% identity among the four aligned sequences. Therefore, the high degree of residue conservation at the *A2*/*A3* interface suggests a functional role for the $\alpha_{49(T)}$ conformation. The invariant residues in Figure 6 are also highly conserved in an alignment of 7 bacterial and 13 archaeal ACS amino acid sequences (*10*).

The archaeal A-cluster-containing subunit resembles α_{49} in that it lacks the N-terminal *A1* domain. Therefore, it is remarkable that 16 of the 20 residues from *A2* and *A3* that interact with *A1* in α_C are conserved in the ACS subunit of the ACDS complex from methanogens (Figure 6). Doukov et al. noted structural similarities between a large fraction of domains *C2* and *C4* of

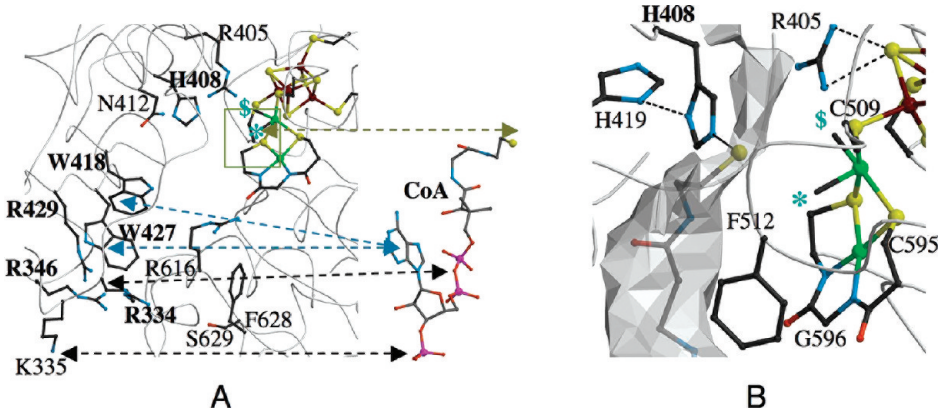

FIGURE 5: Possible interactions of CoA with the narrow cleft formed in $\alpha_{49(T)}$. (A) Arrows indicate the overall complementarity between moieties of CoA (structure taken from PDB deposition 1I12) and putatively protected amino acid residues and reacting metals in the cleft; they connect the 3′-phosphate with K335, adenine with W418/W427, pyrophosphate with R334/R346/R429, and the thiol with Ni_p of the A-cluster. (B) Tentative docking of the cysteamine tail of CoA close to the A-cluster in $\alpha_{49(T)}$ inside a cavity map calculated for an accessible probe radius of 1.4 Å. Apical and equatorial substrate binding sites of the A-cluster Ni_p ion (taken from the superimposed *A3* structure of α_O) are labeled with * and $, respectively.

```
          ----------P----P-FEGE--RK--M-VE-GG------ELVR------I-D-K----G consensus_23
ACS_Mot   --317-KLDLPINFGPAFEGESIRKGDMYVEMGGNRTPAFELVRTVSESEITDGKIEVIG-370
ACS_Ch    --320-DIDLPINFGPAFEGESIRKGDMHVEFGGGKTPSFELVRMVGPDEIEDGKVEVIG-373
ACDS_Met  ----1-MAEFPFEISPMFEGERVRKEGMFVELGGPKSLGLELVRAADMDAIEDDKVTIVG--54
ACDS_Meb  ----1-MAEFPFEISPMFEGERVRKDGMFVELGGPKSMGLELVRAKDLDEIEDDKVTIVG--54
          ..........P.....P.FEGE..RK..M.VE.GG......ELVR......I.D.K....G consensus_1

          PD------G---P------I-G-----D-E-V-ERR-H-F-NY--G--H--QR--W-R- consensus_23
ACS_Mot   PDIDQIPEGSKLPLGILVDIYGRKMQADFEGVLERRIHDFINYGEGLWHTGQRNINWLRV-430
ACS_Ch    PDIDSVEPGGRLPIGIVVDIYGRKMQEDFEPVLERRIHYFTNYGEGFWHTAQRDLTWVRI-433
ACDS_Met  PDLKDMEEGKTYPWAMIFNIGGELVEPDLESVVERRVHDFINYCQGIMHLNQRYDVWMRV-114
ACDS_Meb  PDLKEMEEGKTYPWAMIFNIGGELVEADLESVVERRVHDFVNYCQGIMHLNQRYDVWMRV-
          PD......G...P......I.G.....D.E.V.ERR.H.F.NY..G..H..QR...W.R. consensus_1

          SK----K-------G-------K-E-P-I----QVT--T----V----E-A------RD- consensus_23
ACS_Mot   SKDAVAKGFRFKNYGEILVAKMKEEFPAIVDRVQVTIFTDEAKVKEYMEVAREKYKERDD-490
ACS_Ch    SKEAFAKGARLKHLGQLLYAKFKQEFPSIVDRVQVTIYTDEQKVLELREIARKKYAERDA-493
ACDS_Met  SKDTAGKMDSFEPFGKAVMMLFKTELPFI-EKMQVTFYTGKEEVEKQMELAKEIFKARDA-173
ACDS_Meb  SKDTAAKMDSFDSFGKAVMMLFKTELPFI-EKMQVTFYTDEAEVEKQLEEAKEIFKIRDA-173
          SK....K.......G.......K.E.P.I....QVT..T....V....E.A......RD. consensus_1

          R---L-DE-VD--YGC-LCQSFAP--VC-V-P-R--LCGA--W-D--A-----GP--- consensus_23
ACS_Mot   RMRGLTDETVDTFYSCVLCQSFAPNHVCIVTPERVGLCGAVSWLDAKASYEINHAGPNQP-550
ACS_Ch    RLRELSDEAVDTYYSCLLCQSFAPTHVCIVSPERVGLCGAISWLDAKAAYEINPNGPNQP-553
ACDS_Met  RTKDLHDEDVDVFYGCTLCQSFAPTNVCVVSPDRISLCGAINWFDGRAAAKVDPEGPQFE-233
ACDS_Meb  RTKDLHDEDVDVFYGCTLCQAFAPTNVCVVSPDRISLCGAINWFDGRAAAKVDPEGPQFA-233
          R...L.DE.VD..YGC.LCQSFAP..VC.V.P.R..LCGA..W.D..A.......GP... consensus_1

          --K--------G-----N------S---------------P-TSCGCFE------PE--- consensus_23
ACS_Mot   IPKEGEIDPIKGIWKSVNDYLYTASNRNLEQVCLYTLMENPMTSCGCFEAIMAILPECNG-610
ACS_Ch    IPKEGLIDPVKGQWESFNEYIYKNSQRTIERMNLYTIMEYPMTSCGCFEAIMAYLPELNG-613
ACDS_Met  IAKGDLLDAVTGEYTGVNEIAKKLSSGEFDKIKLHSFFDSPHTSCGCFEVVGFYIPEVDG-293
ACDS_Meb  IEKGELINADTGEYSGVNEIAKKLSSGEYDKINLHSFFEYPHTSCGCFEVVGFYIPEVDG-293
          ..K........G.....N......S...............P.TSCGCFE......PE... consensus_1

          -----R----M-P-G--FST-AG--GGG-Q--GF-GIG-----S-KF--ADGG--R-VW- consensus_23
ACS_Mot   IMITTRDHAGMTPSGMTFSTLAGMIGGGTQTPGFMGIGRTYIVSKKFISADGGIARIVWM-670
ACS_Ch    FMIVNREHSGMTPIGMTFSTLAGMVGGGTQTPGFMGIGKSYIGSRKFVKADGGLARVVWM-673
ACDS_Met  IGWVDREYQGMAPNGIGFSTMAGQTGGGKQIVGFLGIGVNYFYSPKFIQADGGWNRVVWL-353
ACDS_Meb  IGWVNREYQGMAPNGLGFSTMAGQTGGGKQVVGFLGIGVNYFYSPKFIQADGGWNRVVWL-353
          .....R....M.P.G..FST.AG..GGG.Q..GF.GIG.....S.KF..ADGG..R.VW. consensus_1

          P--LK--------------E----D--DKIA-E---T--------L--K-HP--------  consensus_23
ACS_Mot   PKSLKDFLHDEFVRRSVEEGLGEDFIDKIADETIGTTVDEILPYLEEKGHPALTMDPIM--729
ACS_Ch    PKDLKEQLRSIIEERAEEEGLGRDFIDKIADETVGTTVDEVLPFLEEKGHPALSMEPLL--732
ACDS_Met  PSGLKAKI---------DEAIPADLKDKIATENDATDIASLKDFLEAKNHPVVATWAAA--403-(+66)
ACDS_Meb  PAMLKEKI---------AETIPEDIKDKIATENDATDIESLKAFLQEKNHPVVANWASE--403-(+69)
          P..LK.............E....D..DKIA.E...T........L..K.HP......... consensus_1
```

FIGURE 6: Sequence alignment of bacterial and archaeal ACS's. The consensus_23 line highlights residues that are involved in close interactions (<3.8 Å) between *Mot* domains *A2* and *A3*. Colors: gray in α_C and/or α_O, blue in $\alpha_{49(T)}$, and red in all three structures. The consensus_1 line does the same for interactions with *Mot* domain *A1*: gray in α_C, blue in α_O, and red in both. Color codes in sequences: β-strands, green; α-helices, pink; 3_{10}-helices, violet.

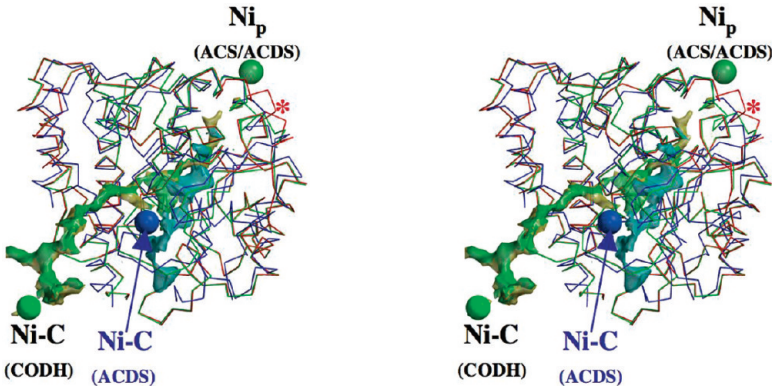

FIGURE 7: Superposition of the C_α backbone of *A1* of ACS_{Mot} α_C (red) and α_O (green) with domains *C2* and *C4* (using the bacterial CODH domain numbering) of $ACDS_{Meb}$ (blue). Corresponding tunnels are shown in yellow, green, and light blue, respectively. $Ni_{p,ACS}$ indicates the location of the catalytic Ni ion of the A-cluster in α_C; the * highlights the nearby flexible helix. Ni−C shows the Ni position in the CODH C-cluster.

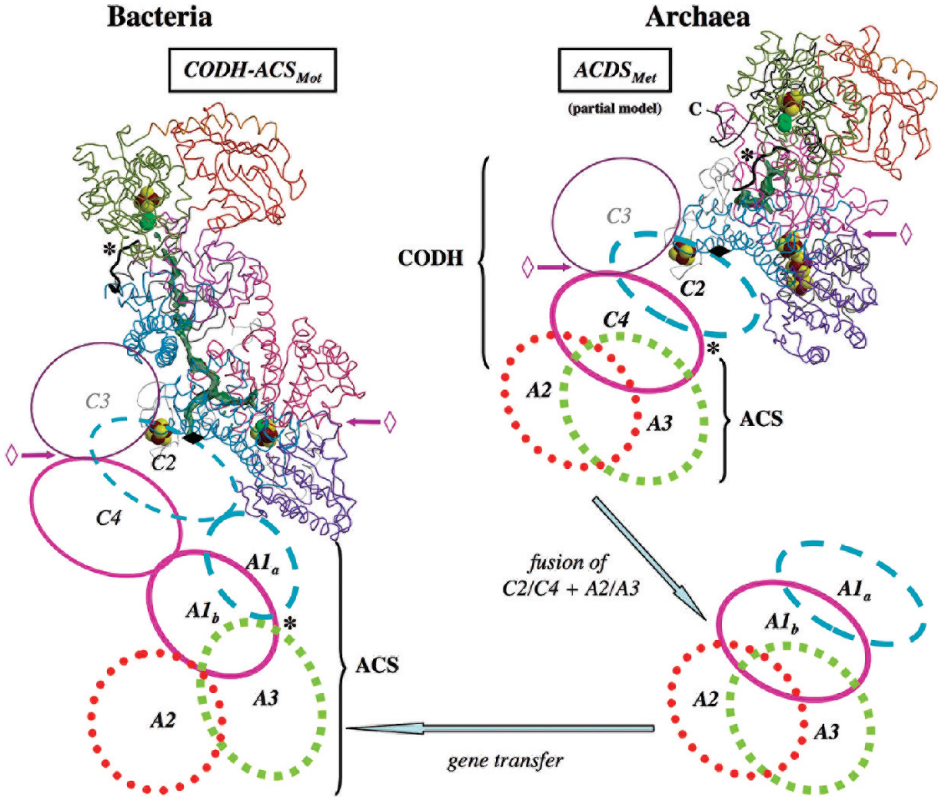

FIGURE 8: Proposed evolutionary relationship of ACS in bacteria and archaea, based on structural comparisons. A tentative model of the complex of the CODH and ACS in the archaeal $ACDS_{Meb}$ is shown with domains numbered as in the bacterial complex. Two of the subunits are shown as C_α traces, using different colors for the various domains. The latter are depicted as ellipses in the other 2-fold symmetry-related subunits. Cluster locations in the top subunits are shown, excluding the D-cluster, which is located on the 2-fold axis (indicated by a closed diamond) that relates subunits; hydrophobic tunnels are depicted in green; asterisks indicate potential ferredoxin binding sites; the C-terminus of one CODH subunit of ACDS is labeled with "C"; the open diamond indicates a pseudo-2-fold symmetry between *C3* and *C4*, perpendicular to the 2-fold axis relating subunits.

CODH and the *A1* domain of ACS in $CODH/ACS_{Mot}$ (*4*). The recently reported structure of the archaeal *Meb* CODH was found to be very similar to its bacterial counterparts, except for its N- and C-terminal regions and the presence of an extra FeS cluster binding domain (*7*). Intrigued by these similarities, we performed a detailed comparison of the available structures (Supporting Information Table S1). We found that $A1_{Mot}$ resembles more the archaeal CODH than the bacterial one. This is indicated by (i) a larger number of superimposed residues (285 vs 217), (ii) a corresponding lower root-mean-square deviation (rmsd) of C_α positions (2.23 vs 2.54 Å), and (iii) a higher percentage of sequence identities (16% vs 12%). When the superposition is carried out separately for two subdomains of *A1*, the statistics are further improved (Supporting Information Table S1). Furthermore, a DALI search (*42*) with $A1_{Mot}$ gives a *Z*-score of 34.1 for the archaeal CODH subunit ($ACDS_{Meb}$-α), compared to a value of 20.8 for the bacterial one ($CODH_{Mot}$-*β*).

The bacterial $ACS/CODH_{Mot}$ *A1* has a tunnel for CO diffusion between the C- and A-clusters and an equivalent tunnel is present in the superimposed archaeal CODH (Figure 7). However, like the tunnel in α_O, it does not reach the surface, being blocked by the helix that in ACS_{Mot} acts as a tunnel gate, allowing a connection between the A- and C-clusters only in α_C (*5*, *20*). If we assume that the archaeal CODH domains that correspond to

C2 and *C4* of their bacterial counterparts have the same tunnel function as ACS_{Mot} domain *A1*, the A-cluster in the superimposed ACDS complex is positioned as in α_C. Accordingly, the distance between the catalytic Ni ions in CODH and ACS would change from 66 Å in the bacterial (α_C) enzyme complex to only about 34 Å in its archaeal counterpart.

We have taken advantage of the high structural (Supporting Information Table S1, Figure 7) and amino acid sequence similarities (Figure 6) among domains of the bacterial and archaeal enzymes to model the relative position of CODH and ACS components in the ACDS complex (Figure 8). Our model predicts that the smaller archaeal ACS interacts with the CODH *C2*/*C4* domains as the bacterial *A2*/*A3* domains interact with ACS_{Mot} *A1* (see also Figure 4). The C_α atom superposition of α_C domain *A1* to $ACDS_{Meb}$-α generates only one potential collision between the rest of the bacterial ACS and the archaeal CODH. It involves Gly327, which aligns with Ser11 of the ACS subunit of ACDS (Figure 6). However, only a small readjustment of the N-terminal region of the archaeal ACS would be required to remove this too short contact. Domain 1 of the archaeal ACS, which corresponds to *A2* in ACS_{Mot}, would also interact with the C-terminal region of one of the CODH subunits (Figure 8). Seven of the 16 residues at the *Mot A1*/*A3* interface are invariant in the superimposed $ACDS_{Meb}$ CODH structure, where they are exposed to solvent (see also Supporting Information Figure S1). This 44% sequence identity is much higher than the overall value of 16% found for the 276 aligned residues (Supporting Information Table S1). Even more strikingly, these conserved residues establish 31 of the 41 contacts ($d < 3.8$ Å) between *A1* and *A3* in α_C. We conclude that the CODH-ACS portion of the ACDS complex shown in Figure 8 is a plausible model for the "closed" form in which there is a continuous tunnel between the A- and C-clusters. Many short (<2 Å) contacts leading to van der Waals collisions are generated when similar superpositions are performed with either α_O or $\alpha_{49(T)}$. Thus, modeling of other putatively functional conformations of the CODH-ACS component of the ACDS complex is not possible with the currently available structures.

DISCUSSION

The structure of $\alpha_{49(T)}$ reported here (Figure 1) shows major differences with previous ACS structures, both in the metal composition of the A-cluster and in the arrangement of domains *A2* and *A3* (Figure 2). Indeed, this is the first structure where the distal site of the A-cluster (M_d) is not occupied by a Ni ion and is empty (Figure 3). This does not prevent the tetrahedral binding of a metal ion heavier than Ni at the proximal labile Ni site (M_p). In this respect $\alpha_{49(T)}$ resembles the CODH-ACS_{Mot} "closed" structures, which show either tetrahedral Zn or Cu bound at the labile Ni M_p site. Since no metal ions were added during the crystallization experiments, the bound Zn or Cu ion must come from either the reagents or the cell extracts used for purification. In fact, the binding of Zn or Cu to the α_{49} subunit in cell extracts would explain why it cannot be activated by the addition of $NiCl_2$ (*14*). Metal heterogeneity greatly complicates the interpretation of spectroscopic studies. In addition to the observed presence of Ni, Cu, and Zn at M_p (*4*, *5*), the results reported here show that A-cluster heterogeneity might also arise from fractions with an empty M_d site. Attempts to generate a $Ni_2Fe_4S_4$ A-cluster by soaking crystals in $NiCl_2$ solutions resulted in crystal cracking and/or loss of diffracting power. Nevertheless, manual model building suggests that only minor changes in the $\alpha_{49(T)}$ structure would be necessary to incorporate Ni at the M_p and M_d sites. For the latter, a small rearrangement of the Cys595-Gly596-Cys597 loop would be required (Figure 5B).

The high percentage of conserved residues between bacterial and archaeal enzymes at the *A2*/*A3* domain interface (Figure 6) suggests that the novel $\alpha_{49(T)}$ conformation, or a closely related one, may be functionally relevant. In terms of A-cluster accessibility, the new structure is intermediate between α_C and α_O. In the former, the A-cluster is connected to the CO-producing C-cluster through a long hydrophobic tunnel. An accessibility analysis (not shown) indicates that in this conformation the active site cannot react with bulky substrates such as CoFeSP or CoA. We have postulated that α_O, in which the connection between the A- and C-clusters is blocked, may be the conformation that accepts a methyl group from CoFeSP (*5*, *20*). Conversely, the novel $\alpha_{49(T)}$ could correspond to the conformation that binds CoA. Indeed, this idea is supported by (i) the presence of tryptophan and arginine residues that could be protected from chemical modification by CoA in the cleft formed between domains *A2* and *A3* (Figure 4), (ii) the electrostatic complementarity between this region and CoA (Figure 4C), and (iii) the corresponding distribution of the adenine, pyrophosphate, and cysteamine moieties of CoA relative to tryptophans, arginines, and the M_p site of the A-cluster, respectively (Figure 5A). Furthermore, in $\alpha_{49(T)}$ His408 is ideally positioned to abstract a proton from CoA-SH before its S^- atom binds to Ni_p (Figure 5B). This is consistent with the prediction (*43*) that a base with a $pK_a \sim 6$ deprotonates CoA.

The structures of α_C and α_O contain another extensive positive patch on the surface of domain 1 (not shown), not far from the A-cluster, involving several arginine residues located around Trp151. According to the results of Shanmugasundaram et al. (*40*, *41*), this region could also bind CoA. However, in α_C the A-cluster is buried in the protein and therefore not accessible for CoA, whereas in α_O access of the cysteamine moiety of the coenzyme to the active site would be blocked by domain *A3*, assuming binding of its adenine and pyrophosphate moieties to Trp151 and surrounding arginines. The binding mode of CoA is likely to be evolutionary conserved. Sequence comparisons (Supporting Information Figure S1 and ref *10*) show that this is not the case for the Trp151 surface region. On the other hand, several crucial residues of the *A2*/*A3* cleft *are* invariant: His408, proposed above to be involved in the deprotonation of CoA-SH, His419, to which His408 is hydrogen-bound (Figure 5B), Trp427, and the nearby Arg334 and Arg429 (Figure 5A). These could be the two arginines that are protected from chemical modification by CoA (*41*). In conclusion, the combination of a large number of observations strongly suggests the involvement of the *A2*/*A3* cleft in CoA binding.

Substantial ACS domain movements during catalysis would explain the reported relatively low rates of acetyl-CoA synthesis ($<10\ s^{-1}$). According to kinetic data, CoA binds to the A-cluster after CH_3^+ and CO (*44*, *45*). This makes sense in a scheme where these two substrates bind to the two available Ni_p coordination sites prior to the migration/insertion reaction that results in acetyl synthesis and that liberates one coordination site for subsequent CoA binding. CoA does not bind to CO-treated ACS (*43*), suggesting that these two substrates might compete for the same binding site and/or that the enzyme conformation is not suitable for coenzyme binding. Similar chemistry involving the sequential binding of three substrates (methyl, CO, and thiol) to a single

nickel ion to produce a thioester has been reported for synthetic Ni(II) complexes (*46*). If our interpretation is correct, CH_3^+, CO, and CoA binding would require the enzyme to adopt conformations similar to α_O, α_C, and $\alpha_{49(T)}$, respectively. In $\alpha_{49(T)}$, two *A2* conserved residues, Arg405 and His408, could respond to changes at the active site and trigger domain movements toward other enzyme conformations (Figures 3 and 5D,E). The order of CH_3^+ and CO binding during catalysis is still controversial (*44*, *45*). If CH_3^+ were to bind Ni_p before CO, a more open α_C conformation would be needed to prevent the collision of the bound methyl group with the enzyme (*20*). Structures of enzyme−substrate complexes and reaction intermediates will be required to determine whether additional conformational changes take place during catalysis. It appears that protein domain movements finely modulate substrate accessibility to the A-cluster by generating suitable interacting surfaces (Figure 4).

Archaeal ACS shows extensive amino acid sequence similarities with *A2* and *A3* from the bacterial enzyme (Figure 6). However, the absence of *A1* in the former implies that the tunnel network between the C- and A-clusters of archaeal ACDS must be different from the one found in bacterial CODH/ACS. Suitable candidates for replacing the tunnel section of bacterial *A1* are two tunnel-containing domains in the CODH portion of a recent $ACDS_{Meb}$-$\alpha_2\varepsilon_2$ crystal structure (*7*). These domains can be superimposed to more than 90% of subdomains $A1_a$ and $A1_b$ (Figure 7, Supporting Information Table S1). Drennan et al. have reported a similar fold for the bacterial $CODH_{Mot}$ domains *C2* and *C4* (*4*), but their resemblance to *A1* is less extensive (Supporting Information Table S1) and they do not contain a tunnel. Although a tunnel *is* present in the same domains in monofunctional CODHs of CO-oxidizing bacteria (*47*, *48*), their similarities to *A1*, reflected by DALI *Z*-scores (*42*) of about 20, are comparable to the value found for the *Mot* enzyme. This *Z*-score is much lower than the value of 34.1, obtained when *A1* and the archaeal *Meb* CODH are compared. Moreover, more than 75% of the residues involved in contacts between *A1* and *A3* in *Mot* α_C are conserved in the aligned sequences of the archaeal domains (Figure 6 and Supporting Information Figure S1). All of these similarities suggest a plausible model for the CODH/ACS interaction in archaeal ACDS that includes a continuous tunnel for CO diffusion between the two active sites, obtained by superposition of *A1* from *Mot* α_C to *C2* and *C4* of $CODH_{Meb}$ (Figure 7).

In the obtained partial model of the ACDS complex (Figure 8), all of the [4Fe-4S] centers of the archaeal CODH are more than 45 Å away from the A-cluster, indicating that there is no direct electron transfer between the two enzymes. Consequently, the reductive activation of the A-cluster should require, like in the bacterial CODH-ACS complex, an external electron source (see also ref *49*). Ferredoxin (Fd) may be the redox partner that activates both bacterial and archaeal enzyme complexes by two successive one-electron reductions (*11*, *50*). It is noteworthy that an *A1* region of $CODH/ACS_{Mot}$ that lies close to the A-cluster and that can be cross-linked with Fd (*51*) is also accessible in the corresponding *C4* region in our partial model of ACDS.

Ni-containing CODH and ACS are considered to be ancient enzymes originally involved in primordial anaerobic carbon fixation pathways (*52*). Their occurrence in both bacteria and archaea may imply that they were already present in the last universal common ancestor (LUCA), but horizontal gene transfer is also a possibility. Domains *C2* and *C4* (bacterial *Mot* enzyme nomenclature) are found in bacterial and archaeal CODH's and hybrid cluster proteins (HCP's) (*53*, *54*) and in *A1* from bacterial ACS (Figure 8). The *C2* domain is involved in extensive contacts with its counterpart in all CODH homodimers, and it has similar contacts with a homologous domain in monomeric HCP's (Supporting Information Figure S2). In CODH's and HCP's there is an additional domain *C3* that is related to *C4* by pseudo-2-fold symmetry (Figure 8, Supporting Information Figure S2). A metal-containing active site is bound at the interface of these two domains: the C-cluster in CODH and the hybrid cluster in HCP. Domains *C2* and *C4* may have originated from a common monomeric ancestral protein of unknown function, possibly binding a simpler metal site. The bacterial ACS domain *A1* lacks *C3*, and consequently, it is not suited to coordinate a metal cluster. However, it is remarkable that its structural similarity to the archaeal CODH *C2* and *C4* domains is comparable to that of the latter to the corresponding bacterial CODH domains (Supporting Information Table S1). Another common feature of CODH, HCP, and bacterial ACS is the presence of a tunnel segment at the *C2*/*C4* interface ($A1_a$/$A1_b$ in ACS; see Figure 8 and Supporting Information Figure S2). In all of these enzymes, except $CODH_{Mot}$, the tunnel continues for an equivalent distance in *C4*. In $CODH_{Mot}$ the tunnel extends inside *A1* instead.

Taken together, our results suggest that bacterial ACS originated from the duplication of the DNA region coding for archaeal CODH *C2* and *C4* domains (generating *A1*) and its fusion to the archaeal ACS gene, consisting of domains *A2* and *A3*. This modification would have allowed for the release of ACS activity from the multienzymatic ACDS methanogenic complex. In this scenario the archaeal enzymes existed before the bacterial ones (see also ref *55*). The *A1*-containing ACS in the CO-tolerant anaerobic thermophilic bacterium *C. hydrogenoformans* is a monomer under high CO concentrations but associates with CODH-III when CO levels are low. This ACS/CODH-III complex, very similar to its counterpart in the acetogenic *Mot*, is postulated to be involved in the Wood−Ljungdahl pathway of CO_2 fixation (*56*). Upon evolution of the acetogenic CODH/ACS complex, most of the tunnel function of the CODH *C4* domain disappeared, presumably to prevent escape of CO. This is different from the situation in the archaeal ACDS multienzyme complex where some CO leakage has been observed (*57*).

CONCLUSIONS

The domain rearrangement found in truncated ACS adds important new information on how protein movements may control the complex catalytic mechanism of acetyl-CoA synthesis. Previously determined closed and open ACS structures appear well suited to bind CO and CH_3^+, respectively. Several lines of evidence suggest that the truncated ACS structure reported here is closely related to the conformation that binds the third substrate, CoA. Further studies, including mutagenesis of selected residues, will be required to establish whether this is indeed the case. The truncated ACS structure has also been used to put forward a scenario for the evolutionary origin of the bacterial ACS from the archaeal ACDS complex.

ACKNOWLEDGMENT

We thank the staff of the BM30A beamline of the ESRF for help with X-ray data collection.

SUPPORTING INFORMATION AVAILABLE

Superposition statistics of bacterial CODH/ACS and archaeal CODH, sequence alignment of bacterial ACS with archaeal CODH, and structure comparison of CODH and HCP. This material is available free of charge via the Internet at http://pubs.acs.org.

REFERENCES

1. Fontecilla-Camps, J. C., and Volbeda, A. (2008) CO dehydrogenase/acetyl CoA synthase, in Handbook of Metalloproteins, online edition (Messerschmidt, A., Ed.) pp 1−16, John Wiley & Sons, DOI: 10.1002/0470028637.met212.
2. Ljungdahl, L. G. (1986) The autotrophic pathway of acetate synthesis in acetogenic bacteria. *Annu. Rev. Microbiol. 40*, 415–450.
3. Wood, H. G. (1991) Life with CO or CO_2 and H_2 as a source of carbon and energy. *FASEB J. 5*, 156–163.
4. Doukov, T. I., Iverson, T. M., Seravalli, J., Ragsdale, S. W., and Drennan, C. L. (2002) A Ni-Fe-Cu center in a bifunctional carbon monoxide dehydrogenase/acetyl-CoA synthase. *Science 298*, 567–572.
5. Darnault, C., Volbeda, A., Kim, E. J., Legrand, P., Vernède, X., Lindahl, P. A., and Fontecilla-Camps, J. C. (2003) Ni-Zn-[Fe_4-S_4] and Ni-Ni-[Fe_4-S_4] clusters in closed and open α subunits of acetyl-CoA synthase/carbon monoxide dehydrogenase. *Nat. Struct. Biol. 10*, 271–279.
6. Jeoung, J.-H., and Dobbek, H. (2007) Carbon dioxide activation at the Ni,Fe-cluster of anaerobic carbon monoxide dehydrogenase. *Science 318*, 1461–1464.
7. Gong, W., Hao, B., Wei, Z., Ferguson, D. J., Tallant, T., Krzycki, J. A., and Chan, M. K. (2008) Structure of the $\alpha_2\varepsilon_2$ Ni-dependent CO dehydrogenase component of the *Methanosarcina barkeri* acetyl-Co decarbonylase/synthase complex. *Proc. Natl. Acad. Sci. U.S.A. 105*, 9558–9563.
8. Volbeda, A., and Fontecilla-Camps, J. C. (2005) Structural bases for the catalytic mechanism of Ni-containing carbon monoxide dehydrogenases. *Dalton Trans. 21*, 3443–3450.
9. Svetlitchnyi, V., Dobbek, H., Meyer-Klaucke, W., Meins, T., Thiele, B., Romer, P., Huber, R., and Meyer, O. (2004) A functional Ni-Ni-[4Fe-4S] cluster in the monomeric acetyl-CoA synthase from *Carboxydothermus hydrogenoformans*. *Proc. Natl. Acad. Sci. U.S.A. 101*, 446–451.
10. Lindahl, P. A., and Graham, D. E. (2007) Acetyl-coenzyme A synthases and nickel-containing carbon monoxide dehydrogenases, in Nickel and its surprising impact in nature, Vol. 2 of Metal ions in life sciences (Sigel, A., Sigel, H., and Sigel, R. K. O., Eds.) pp 357−416, John Wiley & Sons, Chichester, U.K.
11. Ragsdale, S. W., and Pierce, E. (2008) Acetogenesis and the Wood-Ljungdahl pathway of CO_2 fixation. *Biochim. Biophys. Acta 1784*, 1873–1898.
12. Barondeau, D. P., and Lindahl, P. A. (1997) Methylation of carbon monoxide dehydrogenase from *Clostridium thermoaceticum* and mechanism of acetyl coenzyme A synthesis. *J. Am. Chem. Soc. 119*, 3959–3970.
13. Menon, S., and Ragsdale, S. W. (1998) Role of the [4Fe-4S] cluster in reductive activation of the cobalt center of the corrinoid iron-sulfur protein from *Clostridium thermoaceticum* during acetate biosynthesis. *Biochemistry 37*, 5689–5698.
14. Loke, H. K., Tan, X. S., and Lindahl, P. A. (2002) Genetic construction of truncated and chimeric metalloproteins derived from the α subunit of acetyl-CoA synthase from *Clostridium thermoaceticum*. *J. Am. Chem. Soc. 124*, 8667–8672.
15. Gencic, S., and Grahame, D. A. (2003) Nickel in subunit β of the acetyl-CoA decarbonylase/synthase multienzyme complex in methanogens: Catalytic properties and evidence for a binuclear Ni-Ni site. *J. Biol. Chem. 278*, 6101–6110.
16. Gu, W., Gencic, S., Cramer, S. P., and Grahame, D. A. (2003) The A-cluster in subunit β of the acetyl-CoA decarbonylase/synthase complex from *Methanosarcina thermophila*: Ni and Fe K-edge XANES and EXAFS analyses. *J. Am. Chem. Soc. 125*, 15343–15351.
17. Funk, T., Gu, W., Friedrich, S., Wang, H., Gencic, S., Grahame, D. A., and Cramer, S. P. (2004) Chemically distinct Ni sites in the A-cluster in subunit β of the acetyl-CoA decarbonylase/synthase complex from *Methanosarcina thermophila*: Ni L-edge absorption and X-ray magnetic circular dichroism analyses. *J. Am. Chem. Soc. 126*, 88–95.
18. Grahame, D. A., and DeMoll, E. (1996) Partial reactions catalyzed by the protein components of the acetyl-CoA decarbonylase/synthase enzyme complex from *Methanosarcina barkeri*. *J. Biol. Chem. 271*, 8352–8358.
19. Doukov, T. I., Blasiak, L. C., Seravalli, J., Ragsdale, S. W., and Drennan, C. L. (2008) Xenon in and at the end of the tunnel of bifunctional carbon monoxide dehydrogenase/acetyl-CoA synthase. *Biochemistry 47*, 3474–3483.
20. Volbeda, A., and Fontecilla-Camps, J. C. (2004) Crystallographic evidence for a CO/CO_2 tunnel gating mechanism in the bifunctional carbon monoxide dehydrogenase/acetyl coenzyme A synthase from *Moorella thermoacetica*. *J. Biol. Inorg. Chem. 9*, 525–532.
21. Vernède, X., and Fontecilla-Camps, J. C. (1999) A method to stabilize reduced and/or gas-treated protein crystals by flash-cooling under a controlled atmosphere. *J. Appl. Crystallogr. 32*, 505–509.
22. Diederichs, K., McSweeney, S., and Ravelli, R. B. (2003) Zero-dose extrapolation as part of macromolecular synchrotron data reduction. *Acta Crystallogr. D59*, 903–909.
23. Kabsch, W. (2001) in International tables for crystallography, Vol. F. Crystallography of Biological Macromolecules (Rossmann, M. G., and Arnold, E., Eds.) pp 218−225, Kluwer Academic Publishers, Dordrecht.
24. Read, R. J. (2001) Pushing the boundaries of molecular replacement with maximum likelihood. *Acta Crystallogr. D57*, 1373–1382.
25. Storoni, L. C., McCoy, A. J., and Read, R. J. (2004) Likelihood-enhanced fast rotation functions. *Acta Crystallogr. D60*, 432–438.
26. McCoy, A. J., Grosse-Kunstleve, R. W., Storoni, L. C., and Read, R. J. (2005) Likelihood-enhanced fast translation functions. *Acta Crystallogr. D61*, 458–464.
27. Murshudov, G. N., Vagin, A. A., and Dodson, E. J. (1997) Refinement of macromolecular structures by the maximum-likelihood method. *Acta Crystallogr. D53*, 240–255.
28. Collaborative Computational Project Number 4 (1994) The CCP4 suite: programs for protein crystallography. *Acta Crystallogr. D50*, 760–763.
29. Winn, M. D., Isupov, M. N., and Murshudov, G. N. (2001) Use of TLS parameters to model anisotropic displacements in macromolecular refinement. *Acta Crystallogr. D57*, 122–133.
30. Roussel, A., and Cambillaud, C. (1991) The Turbo-Frodo graphics package, in Silicon Graphics Geometry Partners Directory , Vol. 81, Silicon Graphics Corp., Mountain View, CA.
31. Chabrière, E., Volbeda, A., Fontecilla-Camps, J. C., Roth, M., and Charon, M. H. (1999) Combination of methods used in the structure solution of pyruvate:ferredoxin oxidoreductase from two crystal forms. *Acta Crystallogr. D55*, 1546–1554.
32. Kraulis, P. J. (1991) MOLSCRIPT: a program to produce both detailed and schematic plots of protein structures. *J. Appl. Crystallogr. 24*, 946–950.
33. Merritt, E. A., and Bacon, D. J. (1997) Raster3D: photorealistic molecular graphics. *Methods Enzymol. 277*, 505–524.
34. Lawrence, M. C., and Bourke, P. (2000) CONSCRIPT: a program for generating electron density isosurfaces for presentation in protein crystallography. *J. Appl. Crystallogr. 33*, 990–991.
35. Baker, N. A., Sept, D., Joseph, S., Holst, M. J., and McCammon, J. A. (2001) Electrostatics of nanosystems: application to microtubules and the ribosome. *Proc. Natl. Acad. Sci. U.S.A. 98*, 10037–10041.
36. Dolinsky, T. J., Nielsen, J. E., McCammon, J. A., and Baker, N. A. (2004) PDB2PQR: an automated pipeline for the setup, execution, and analysis of Poisson-Boltzmann electrostatics calculations. *Nucleic Acids Res. 32*, W665–W667.
37. Ponder, J. W., and Case, D. A. (2003) Force fields for protein simulations. *Adv. Protein Chem. 66*, 27–85.
38. Bas, D. C., Rogers, D. M., and Jensen, J. H. (2008) Very fast prediction and rationalization of pK_a values for protein-ligand complexes. *Proteins 73*, 765–783.
39. Keire, D. A., Robert, J. M., and Rabenstein, D. L. (1992) Microscopic protonation equilibria and solution conformations of coenzyme A and coenzyme A disulfides. *J. Org. Chem. 57*, 4427–4431.
40. Shanmugasundaram, T., Kumar, G. K., and Wood, H. G. (1988) Involvement of tryptophan residues at the coenzyme A binding site of carbon monoxide dehydrogenase from *Clostridium thermoaceticum*. *Biochemistry 27*, 6499–6503.
41. Shanmugasundaram, T., Kumar, G. K., Shenoy, B. C., and Wood, H. G. (1989) Chemical modification of the functional arginine residues of carbon monoxide dehydrogenase from *Clostridium thermoaceticum*. *Biochemistry 28*, 7112–7116.
42. Holm, L., Käärliäinen, S., Rosenström, P., and Schenkel, A. (2008) Searching protein structure bases with DaliLite v.3. *Bioinformatics 24*, 2780–2781.
43. Wilson, B. E., and Lindahl, P. A. (1999) Equilibrium dialysis study and mechanistic implications of coenzyme A binding to acetyl coenzyme A synthase/carbon monoxide dehydrogenase from *Clostridium thermoaceticum*. *J. Biol. Inorg. Chem. 4*, 742–748.

44. Tan, X., Surovtsev, I. V., and Lindahl, P. A. (2007) Kinetics of CO insertion and acetyl group transfer steps and a model of the acetyl coenzyme A synthase catalytic mechanism. *J. Am. Chem. Soc. 128*, 12331–12338.
45. Seravalli, J., and Ragsdale, S. W. (2008) Pulse-chase studies of the synthesis of acetyl-CoA by carbon monoxide dehydrogenase/acetyl-CoA synthase. *J. Biol. Chem. 283*, 8384–8394.
46. Stavropoulos, P., Muetterties, M. C., Carrié, M., and Holm, R. H. (1991) Structural and reaction chemistry of nickel complexes in relation to carbon-monoxide dehydrogenase - a reaction system simulating acetyl-coenzyme-A synthase reactivity. *J. Am. Chem. Soc. 113*, 8485–8492.
47. Dobbek, H., Svetlitchnyi, V., Gremer, L., Huber, R., and Meyer, O. (2001) Crystal structure of a carbon monoxide dehydrogenase reveals a [Ni-4Fe-5S] cluster. *Science 293*, 1281–1285.
48. Drennan, C. L., Heo, J., Sintchak, M. D., Schreiter, F., and Ludden, P. W. (2001) Life on carbon monoxide: X-ray structure of *Rhodospirillum rubrum* Ni-Fe-S carbon monoxide dehydrogenase. *Proc. Natl. Acad. Sci. U.S.A. 98*, 11973–11978.
49. Maynard, E. L., Tan, X., and Lindahl, P. A. (2004) Autocatalytic activation of acetyl-CoA synthase. *J. Biol. Inorg. Chem. 9*, 316–322.
50. Gencic, S., and Grahame, D. A. (2008) Two separate one-electron steps in the reductive activation of the A cluster in subunit β of the ACDS complex in *Methanosarcina thermophila*. *Biochemistry 47*, 5544–5555.
51. Shanmugasundaram, T., T., and Wood, H. G. (1992) Interaction of ferredoxin with carbon monoxide dehydrogenase from *Clostridium thermoaceticum*. *J. Biol. Chem. 267*, 897–900.
52. Russell, M. J., and Martin, W. (2004) The rocky roots of the acetyl-CoA pathway. *Trends Biochem. Sci. 29*, 358–363.
53. Cooper, S. J., Garner, C. D., Hagen, W. R., Lindley, P. F., and Bailey, S. (2000) Hybrid-cluster protein (HCP) from *Desulfovibrio vulgaris* (Hildenborough) at 1.6 Å resolution. *Biochemistry 39*, 15044–15054.
54. Aragão, D., Mitchell, E. P., Frazão, C. F., Carrondo, M. A., and Lindley, P. F. (2008) Structural and functional relationships in the hybrid cluster protein family: structure of the anaerobically purified hybrid cluster protein from *Desulfovibrio vulgaris* at 1.35 Å resolution. *Acta Crystallogr. D64*, 665–674.
55. Lindahl, P. A., and Chang, B. (2001) The evolution of acetyl coenzyme A synthase. *Orig. Life Evol. Biosph. 31*, 403–434.
56. Wu, M., Ren, Q., Durkin, A. S., Daugherty, S. C., Brinkac, L. M., Dodson, R. J., Madupu, R., Sullivan, S. A., Kolonay, J. F., Nelson, W. C., Tallon, L. J., Jones, K. M., Ulrich, L. E., Gonzalez, J. M., Zulin, I. B., Robb, F. T., and Eisen, J. A. (2005) Life in hot carbon monoxide: the complete genome sequence of *Carboxydothermus hydrogenoformans* Z-2901. *PLoS Genet. 1*, 563–574.
57. Eikmann, B., Fuchs, G., and Thauer, R. K. (1983) Formation of carbon monoxide from CO_2 and H_2 by *methanobacterium thermoautotrophicum*. *Eur. J. Biochem. 146*, 149–154.